Distinct Photochemistry in Glycine Particles Mixed with Different Atmospheric Nitrate Salts

Zhancong Liang[1,2], Zhihao Cheng[1], Ruifeng Zhang[1,2], Yiming Qin[1], Chak K. Chan[1, 3*]

[1]School of Energy and Environment, City University of Hong Kong, Hong Kong, China
[2]City University of Hong Kong Shenzhen Research Institute, Shenzhen, China
[3]Division of Physical Science and Engineering, King Abdullah University of Science and Technology, Thuwal, 23955-6900, Saudi Arabia

Correspondence to: Chak K. Chan (chak.k.chan@cityu.edu.hk; chak.chan@kaust.edu.sa)

Abstract. Particulate Free amino acids (FAAs) are essential components of organonitrogen that have critical climate impacts, but they are usually considered stable end products from protein degradation. In this work, we investigated the decay of glycine (GC) as a model FAA under photolysis of different particulate nitrate salts using an in-situ micro-Raman system. Upon changes of the relative humidity (RH) cycle between 3 and 80% RH, ammonium nitrate (AN)+GC mixed particles did not exhibit any phase change, whereas sodium nitrate (SN)+GC mixed particles crystallized at 60% and deliquesced at 82% RH. Under light illumination at 80% RH, AN+GC particles showed almost no spectral changes, while rapid decays of glycine and nitrate were observed in SN+GC particles. The interactions between nitrate and glycine in AN+GC particles suppressed crystallization but also hindered nitrate photolysis and glycine decay. On the other hand, glycine may form a complex with Na$^+$ in deliquescent SN+GC particles and allow unbonded nitrate to undergo photolysis and trigger glycine decay, though nitrate photolysis was greatly hindered upon particle crystallization. Our work provides insights into how FAAs may interact with different nitrate salts under irradiation and lead to distinct decay rates, which facilitates further investigations on their atmospheric lifetime estimation.

1 Introduction

Free amino acids (FAAs) are essential components of atmospheric particles with wide sources, including direct bio-emission, degradation of proteinaceous materials, and biomass burning (Ren et al., 2018; Matos et al., 2016; Zhu et al., 2021; Li et al., 2022a; Liu et al., 2017a). The concentrations of FAAs in terrestrial and marine near-surface atmospheres generally range from a few to several hundred ng m^{-3} (Helin et al., 2017; Matos et al., 2016). FAAs play important roles in the climate-related properties of atmospheric particles, such as hygroscopicity and cloud condensation nuclei (CCN) activity (Chan et al., 2005; Kristensson et al., 2010; Marsh et al., 2017), and atmospheric nitrogen cycling (Mopper et al., 1987). Besides, FAAs support the biological activity in the aerosol particles (Helin et al., 2017) and impact human health after inhalation (Hu et al., 2020). While the importance of atmospheric FAAs was well-recognized, previous atmospheric studies mainly focused on the regional and seasonal variations of the abundance of particulate FAAs (Ren et al., 2018; Helin et al., 2017; Song et al., 2017). FAAs were suggested as the stable end products of the degradation of protein (Li et al., 2022a). However, a few studies have reported

the reactivity of atmospheric FAAs with dicarbonyls, to form light-absorbing compounds via oligomerization under dark (De Haan et al., 2011; Haan et al., 2009). The photochemical evolution of FAAs remains less explored.

Nitrate is ubiquitous in atmospheric particles (Chan et al., 2008), and it can generate various oxidants, including OH radicals, via photolysis (Gen et al., 2022; Scharko et al., 2014; Benedict et al., 2017). Oxidants from particulate nitrate photolysis could oxidize gaseous precursors to secondary inorganic and organic aerosols (Gen et al., 2022; Gen et al., 2019; Zhang et al., 2021; Zhang et al., 2022) and change the morphology of the particles (Liang et al., 2021). Correlation analysis of field measurements suggests that particulate FAAs and nitrate could be from the same sources (Xu et al., 2019; Gao et al., 2021), and there were also laboratory studies on the hygroscopicity of FAAs-nitrate mixed particles (Ashraf et al., 2021; Wang et al., 2018). While external oxidants such as gaseous ozone and OH radicals need to diffuse across the interfacial layers, nitrate photolysis generates oxidants inside the particles to oxidize the particulate components (Liang et al., 2021). These characteristics make effective FAAs oxidation triggered by nitrate photolysis possible. However, it is unclear how FAAs would chemically evolve under nitrate photolysis, though it is well-known that OH radicals can react with FAAs in water treatment research (Berger et al., 1999; Acero et al., 2000). Recently, Wen et al. (2022) demonstrated that aqueous OH oxidation could be a significant sink of atmospheric FAAs. Nevertheless, while these results were helpful to dilute aqueous systems, the reactions in the particle phase could be different due to the elevated concentrations that facilitate molecular interactions. Specifically, glycine (GC), which is the most abundant FAA in atmospheric particles (mole ratio of GC to total FAAs = 0.17-0.49) (Li et al., 2022a; Ren et al., 2018; Song et al., 2017; Zhang et al., 2003; Zhu et al., 2020), could bind with atmospheric-relevant inorganics such as sulfate and nitrate (Ashraf et al., 2021). The phase state of the particles can also play an essential role in nitrate photolysis (Liang et al., 2021; Gen et al., 2022).

In this paper, we first performed relative humidity (RH)-cycle to characterize the phase transition behavior of mixed particles of ammonium nitrate (AN) and glycine as well as sodium nitrate (SN) and glycine. Then, we examined the photochemistry of glycine triggered by the photolysis of AN and SN at different RHs. The phase transition behaviors of AN+GC and SN+GC mixed particles and the kinetics of glycine decay under UV illumination are significantly different.

2 Experimental

2.1 Photochemical aging of the droplets

Mixed solutions (1% wt) of AN (>99%, Sigma-Aldrich) or SN (>99%, Arcos) and glycine (Biological analysis level, Chemcruz™) were prepared in ultrapure water (Milli-Q). We used a mole ratio of 1:1 for glycine and nitrate in all our experiments. Mixed solutions were atomized using a piezoelectric particle generator (model 201, Uni-Photon Inc.) coupled with a quartz tip (Micro-Fab, orifice diameter = 80 μm). Droplets were deposited on a hydrophobic fluorocarbon substrate (model 5793, YSI Inc.) and placed in an aerosol flow cell (Liang et al., 2021; Liang et al., 2022b). The flow cell has two

windows for in situ Raman analysis (top) and ultraviolet (UV) illumination (bottom). The schematic of the experimental setup is shown in the Supporting Information (Figure S1). RH inside the flow cell was controlled by mixed dry and wet synthetic air (Linde) and monitored by a digital RH sensor (HC2-C05, ROTRONIC AG, Switzerland). The deposited droplets were

70 photolyzed for 8 h using a 300 nm light-emitting diode (LED) lamp (M300L4, Thorlabs), through the bottom window of the flow cell. The photon flux received by deposited particles in the flow cell was determined to be 1.2×10^{15} photons cm^{-2} s^{-1} by 2-nitrobenzaldehyde (2NB, >99.0%, Acros Organics). A detailed description can be found in our previous work (Liang et al., 2021). The effective incident light flux (photons cm^{-2} s^{-1}) used in our study was comparable to that received by nitrate in the atmosphere on a typical clean day.

75

2.2 In-situ Raman and microscopic characterization

A Raman spectrometer (EnSpectr R532, EnSpectr) with a 20−30 mW 532 nm laser and holographic diffraction grating with 1800 grooves/mm was used to characterize the particle *in-situ* during phase transition behavior measurement and photoreactions of the particles. The Raman spectrometer was coupled with an optical microscope (CX41, Olympus) to acquire

80 Raman spectra at 100−4000 cm^{-1} at a resolution of 4 cm^{-1}. A 50× objective lens with a numerical aperture of 0.35 (SLMPLN50X, Olympus) was used to guide the laser onto the sample. For the phase transition measurements, we evaporated and then humidified the droplets by decreasing and increasing the RH gradually. Images of the particles were captured, and the Raman spectra were recorded after equilibrium was reached. The size of the equilibrated droplets at 80% RH were 41±15 µm. The in-situ Raman analysis focused on single particles of ~40 µm, while approximately 1300 particles were used for off-

85 line analysis (will be discussed later). Particle composition during photoreactions was monitored using Raman measurement every hour for 8 hours. The integration time for each spectrum is 5 s. Glycine absorbs light at below 260 nm, but it can form light-absorbing meso-clusters in droplets and trigger photosensitization to degrade themselves at 532 nm, the Raman excitation wavelength in our experiments (Ishizuka et al., 2023). However, this mechanism plays a minor role in our system as no glycine decay in GC droplets without nitrate at 80%RH was found.

90

2.3 Off-line chemical analysis of the particle extract

Particle-loaded substrates were extracted using 1 mL MilliQ water after photoreactions. The water extract was analyzed by ion chromatography (IC). The IC protocol was the same as our previous work (Liang et al., 2022c). After equilibrating at 80% RH, the initial particle pH was measured by a pH indicator combined with RGB-based colorimetric analyses using a model

95 of $G−B$ (G minus B) vs. pH^2, according to Craig et al. (Craig et al., 2018). The particles were considered at equilibrium when the size became unchanged (±2%) for 30 min. The nitrate and glycine concentrations were obtained according to Eq. 1, where "a" is the scaling factor determined by calibration, and A refers to the integrated area of the corresponding peak using Gaussian fitting (Igor Pro 8). The wavenumber ranges used for integration were 850-950 cm^{-1} for glycine and 980-1100 cm^{-1} for nitrate, respectively.

100 $[X]_{particle} = a \times (A(X) / A(OH)_{3400cm^{-1}})$ ⟶ X is nitrate, glycine ⟶ (1)

2.4 Estimation of nitrate photolysis rate constant and percentage glycine decay

The maximum RH reached in the flow cell was 96%, which yields a solute concentration in particles higher than 1 M. Thus, data of diluted systems (0.01, 0.1, and 0.5 M) were obtained from kinetic measurements of aqueous solutions. The schematic of the custom-made aqueous reactor is shown in Figure S2. Synthetic air was introduced to the aqueous reactor at 0.1 L/min. AN+GC and SN+GC solution (0.01, 0.1, or 0.5 M) were added to the aqueous reactor and illuminated by 300 nm LED through a quartz window on the top of the reactor. The photon flux received by the solution was determined to be 0.7×10^{15} photons cm^{-2} s^{-1} by 2-NB, ~60% of that flux found for deposited particles in the flow cell. Therefore, we sampled the aliquots from the aqueous solution after 13.3 h of irradiation. After sampling, the glycine concentration was immediately determined using the pre-column derivatization HPLC method described by Matsumoto et al. (2021). The nitrate concentration was determined by IC.

The apparent nitrate photolysis rate constant J (s^{-1}) was estimated as Eq. 2. J depends on the light intensity, quantum yield, and absorption cross-section of nitrate (George et al., 2015).

$$\frac{d[NO_3^-]}{dt} = -J \times [NO_3^-] \tag{2}$$

This is a low estimate of J since glycine oxidation likely generates secondary nitrate (Berger et al., 1999). We estimated the percentage GC decay to indicate the effectiveness of the decay under different conditions based on [GC] measured before and after irradiation (after 8 h for deposited particles and 13.3 h for solutions). The percentage GC decay in crystalline SN+GC particles was estimated directly by the GC peak as the water peak was not available.

2.5 Estimation of the water to glycine mole ratio

Though still under debate, the water-to-glycine mole ratio was reported to play a crucial role in affecting the configuration of glycine (Aikens et al., 2006; Tortonda et al., 1996). Herein, we estimate the water-to-glycine mole ratio in AN+GC and SN+GC particles and discuss the potential form of glycine, which may play a role in photochemistry.

$$GF = \frac{V_{wet}}{V_{dry}} = \frac{(m_w + m_{dry})/\rho_{wet}}{\frac{m_{dry}}{\rho_{dry}}} = \left(1 + \frac{m_w}{m_{dry}}\right) \times \frac{\rho_{dry}}{\rho_{wet}} = (1 + \frac{M_w}{M_{dry}} \times \frac{n_w}{n_{dry}}) \times \frac{\rho_{dry}}{\rho_{wet}} \tag{3}$$

$$GF = \frac{V_{wet}}{V_{dry}} = \frac{(d_{wet})^3}{(d_{dry})^3} \tag{4}$$

GF is the volumetric growth factor (i.e., the volume ratio of a wet droplet to dry particles at specific RH), and V, m, ρ, n, M, and d represent the volume, mass, density, mole number, molar mass and diameter of the particles, respectively. The subscripts dry, wet, and w denote dry particles (i.e., solutes), wet particles, and water, respectively. Note that the estimation of GF using equation 4 assumes spheric particles on the hydrophobic substrate, d_{dry} was estimated by averaging two measured diameters from orthogonal directions. For an initially non-spherical particle to form a droplet upon RH increase, the estimation of GF by equation 4 would be a slight overestimation (Matsumura et al., 2007). Then, the water-to-glycine mole ratio (WGR) can be solved by:

$$WGR = 2 \times \frac{n_w}{n_{dry}} = 2 \times \left[\frac{(d_{wet})^3}{(d_{dry})^3} \times \frac{\rho_{wet}}{\rho_{dry}} - 1\right] \times \frac{M_{dry}}{M_w} \qquad (5)$$

The mean molar mass of glycine and the nitrate salts was used as M_{dry}. ρ_{dry} of SN+GC particles was available in the literature
(Suresh et al., 2010), while ρ_{dry} of AN+GC particles and ρ_{wet} of both particles were estimated based on the simple volume
additivity rule (Equation 6) (Ha et al., 1999; Tang, 1997). ρ_{GC}, $\rho_{AN,}$ and ρ_{SN} were the densities of pure aqueous solutions at the
total solute mass fraction X of the mixed solution obtained from the literature (Venkatesu et al., 2007) and E-AIM prediction
(Clegg et al., 1998).

$$\frac{1}{\rho_{wet}} = \frac{X_{GC}}{\rho_{GC}} + \left(\frac{X_{AN}}{\rho_{AN}} \ or \ \frac{X_{SN}}{\rho_{SN}}\right) \qquad (6)$$

3 Results and discussions

3.1 Phase transition behavior of nitrate-glycine mixed particles

We first examined the phase transition behavior of the nitrate-glycine mixed particles without UV illumination. Figure 1 shows
the images and Raman spectra of AN+GC and SN+GC particles undergoing an evaporation-humidification cycle. The black
line in Figure 1b shows the Raman spectra of an AN+GC mixed droplet at 85% RH. The $v(NO_3^-)$ peaks are at ~730 cm^{-1} and
~1040 cm^{-1} (Ling et al., 2007). The C-C stretching and C-N stretching peaks are located at ~890 cm^{-1} (Socrates, 2004). In
1300-1450 cm^{-1}, there are overlapping peaks from C-H vibration in different chemical environments. Peaks at 2970 cm^{-1} and
3020 cm^{-1} show the antisymmetric and symmetric stretching of CH_2, respectively. The two broad peaks at 3250 cm^{-1} and 3450
cm^{-1} are from the stretching of OH, indicating the presence of liquid water (Furić et al., 1992). The $v(NH_4^+)$ also contributed
to the peak at 3250 cm^{-1}.

Upon RH decrease from 85% to 3%, the AN+GC particle shrank but remained spherical, suggesting the particle gradually lost
water and became dry amorphous solids (Figure 1a). Crystallization did not occur since there was no sudden decrease in the
full width at half maxima (FWHM) of the nitrate and glycine peaks (Liang et al., 2021; Surovtsev et al., 2012; Liang et al.,
2022a). Besides, the 3450 cm^{-1} peak diminished, suggesting that the particle lost water without phase transition, consistent
with the literature (Wang et al., 2022). Although some studies reported an absence of efflorescence RH (ERH) in pure AN
(Zuend et al., 2011; Lightstone et al., 2000), the ERH of pure GC was 61.7% (Wang et al., 2022). Adding crystallizable
organics such as succinic acid to AN would also promote its crystallization (Lightstone et al., 2000). The absence of a phase
transition in the AN+GC particles can be attributed to the chaotropic nature of AN, which results in the "salting-in" effect of
glycine and the gradual but not abrupt evaporation of water (Ashraf et al., 2021), without crystallization. As an amino acid,
GC has a proton-donating carboxyl (COOH) group and a proton-accepting amino (NH_2) group. The latter can form hydrogen
bonding with nitrate to suppress crystallization (Wang et al., 2022). This was supported by the FWHM increases of GC and
nitrate peaks as RH decreased (Figure S3) due to intensified molecular interaction. The particles are likely dehydrated at 3%

RH due to the absence of OH peaks from 3200 to 3500 cm^{-1}. As RH increased, the particle took up water again and grew. There was no spectral change other than the increase of the O-H peak at 3450 cm^{-1} (Guo et al., 2010).

165

For the SN+GC particle, the particle size decreased as RH decreased from 84% to 60% (Figure 1c). The black line in Figure 1d shows the Raman spectrum of an SN+GC mixed droplet at 84% RH, which is almost identical to that of an AN+GC mixed droplet at 85% RH. Interestingly, different from AN+GC particles, a phase transition from liquid to crystalline solid was observed at 54% RH. The Raman spectra show a redshift of the nitrate peak at 730 cm^{-1} to 710 cm^{-1} and a blue shift of the

170   1046 cm^{-1} peak to 1051 cm^{-1}, attributable to the formation of glycine-sodium nitrate crystal (GSN) (Figure S4)(Gujarati et al., 2015). Two new peaks are attributed to the -NH_3^+ rocking mode at 1100 cm^{-1} after crystallization, likely due to the more restricted vibration in the crystalline lattice than in the aqueous droplet (Jentzsch et al., 2013). The FWHM of the CH_2 peaks at 1300 cm^{-1} and 3020 cm^{-1} also decreased after crystallization. As RH further decreased to 3%, no noticeable change in appearance was observed. The SN+GC crystal returned to a droplet at 82% RH after humidification.

175

3.2 Photochemistry of glycine with different nitrate salts

The different phase transition behaviors observed in AN+GC and SN+GC particles reflect the role of molecular interaction in determining the physicochemical properties of the particles. To examine if such interactions could play a role in the chemical reactivity of the particles, we exposed the AN+GC and SN+GC particles to UV irradiation at 80% RH.

180

The Raman spectral characteristics of AN+GC particles only show slight changes from 0 to 8 h irradiation (Figure 2a). Offline IC analysis also shows no new product formed (Figure S5). However, the spectra of SN+GC particles show apparent changes upon light irradiation. Overall, glycine peaks, including C-N/C-C (890 cm^{-1}) and CH_2 (1325 cm^{-1}, 1425 cm^{-1}, 2970 cm^{-1} and 3020 cm^{-1}) (Kumar et al., 2005), decreased but peaks at 920 cm^{-1} (C-C) and 1350 cm^{-1} (C-O) attributable to acetate and formate,

185   respectively, emerged (Figure S5, S6) (Zhang et al., 2021). The rising peaks at 1350 and 2925 cm^{-1} correspond to amide and ammonia or/and amine (Philipsen et al., 2013; Socrates, 2004). Besides, nitrite was also found in the particle extracts using IC. Nitrate photolysis directly generates HNO_2/NO_2^- (Gen et al., 2022), and the reaction between the two other nitrate photolysis products, NO_2 and OH^-, would also form nitrite (Pei et al., 2022).

190   ### 3.3 Nitrate photochemistry of AN+GC and SN+GC particles

The efficiencies of nitrate photolysis in the two mixed systems were different. The fitted apparent nitrate photolysis rate constant of SN+GC particles at 80% RH was 9×10^{-6} s^{-1} ($R^2 = 0.95$), 4.5-folds higher than that of AN+GC particles (Figure S7). The nitrate photolysis rate constant in SN+GC particles was comparable to SN particles without glycine (1.2×10^{-5} s^{-1}), which indicates that glycine has a minor suppression effect on SN photolysis. The faster nitrate photolysis in SN+GC particles

195   likely contributed to the faster glycine decay, and the molecular interactions may explain the discrepancy in nitrate photolysis rate constant between SN+GC and AN+GC particles.

For instance, amino acid nitrate can form through (water-mediated) hydrogen bonding between nitrate from AN and the protonated amino group of glycine (Figure 3a) (Wang et al., 2022; Ashraf et al., 2021). As a result, the amino acids and nitrate ions in the droplet are bounded in an extensive three-dimensional hydrogen-bonded matrix (Wang et al., 2022), in which nitrate photolysis could be hindered (Vimalan et al., 2010). We envision that such interactions exist in our AN+GC system. On the other hand, the COO^- of glycine can bind with SN via Na^+ directly to form a bidentate complex (Figure 3a) (Moision et al., 2002; Aziz et al., 2008; Selvarani et al., 2022), leaving nitrate unbonded. The nitrate peak in SN+GC particles split into two (Figure 3b). One has the same Raman shift as nitrate in AN+GC, likely bonded nitrate, while the other peak at 1046 cm^{-1} was attributable to unbonded aqueous nitrate (Liang et al., 2022a), which can undergo photolysis to form a wealth of oxidants that lead to glycine decay (Figure 3a). The single symmetric nitrate peak, small J, and minor glycine decay of AN+GC particles suggested a negligible fraction of unbonded nitrate. However, we also note that the exact molecular configuration in concentrated particles can be much more complicated than the illustrative example shown in Figure 3a. Detailed investigations of quantum chemistry and molecular dynamic simulation with appropriate parameterization for non-ideal solutions are required.

One would expect that these effects are more evident at lower RH (but before crystallization), with higher solute concentrations and fewer water molecules. Figure 4a shows the percentage GC decay after irradiation as a function of the initial solute concentrations. At 0.01M, the percentage GC decay is approximately 5% in both AN+GC and SN+GC solutions (Figure 4a). However, as the initial solute concentration increased from 0.01 M to ~7.6 M, the percentage GC decay in SN+GC particles increased by more than one order of magnitude to 70%, while that of the AN+GC particles remained small. The apparent nitrate photolysis rate constant J shows a good correlation with the percentage GC decay ($R^2 = 0.99$, Figure 4b), which suggests that nitrate photolysis is the key driver for the glycine decay.

The different reactivity of glycine between SN+GC and AN+GC particles may also contribute to the distinct photochemistry. For instance, glycine can be ionized into different forms according to the local conditions, including cationic, zwitterionic, and anionic of different reactivities (Aikens et al., 2006). Zwitterionic denotes the charge-separated form amino acids in aqueous solutions and in crystalline states (e.g., NH_3^+–CH_2–COO^-). Several possible zwitterionic conformers of glycine have been proposed with the addition of 1-3 water molecules (Krauklis et al., 2020). The rate of anionic glycine reacting with OH radicals is 2-orders of magnitude higher than that of zwitterionic glycine (Berger et al., 1999; Buxton et al., 1988), while that of zwitterionic glycine is several times higher than cationic glycine. These differences were due to the increased energy barriers for oxidation upon protonation (Wen et al., 2022). However, the protonation constants of glycine in concentrated solution were difficult to define. Qualitatively, a possible lower degree of glycine protonation in SN+GC particles than AN+GC particles might enhance the reactivity of glycine.

We also note that the initial water-to-glycine mole ratios were higher for AN+GC particles (6) than SN+GC particles (2), and sodium has higher hydration number (6)(Medoš et al., 2019) than ammonium (4)(Guo et al., 2020). Therefore, the availability of free water in AN+GC particles is likely higher than in SN+GC particles. This could affect the configuration of glycine dimers or trimers, such as the possible complexation or charge interactions between the anionic carboxylate and the cationic -
235 NH_3^+ groups. These factors could also modulate the photo-reactivity of glycine.

Though no phase transition occurred at RH below 60%, the percentage GC decay in AN+GC particles was very small (Figure 4c). On the other hand, SN+GC particles crystallized at 50%, and the percentage GC decay after 8 h irradiation became <5%, much smaller than that at 80% RH (Figure 4c). Such reduction in glycine decay was likely due to the ineffective photolysis of
240 nitrate in the crystalline lattices (Asher et al., 2011). The crystalline lattices greatly constrain the diffusion of nitrate photolysis products and facilitate their recombination to form nitrate, resulting in a very low photolysis quantum yield.

4 Atmospheric implications

This work showed the distinct decay characteristics of glycine as a model FAA in AN and SN particles under the light. AN+GC particles did not crystalize at RH as low as 3%, while SN+GC did at 50-60% RH. On the other hand, glycine in AN+GC
245 particles exhibited a much slower decay than in SN+GC particles under UV irradiation. A plausible explanation was the water-mediated bonding between nitrate and GC in AN+GC particles that suppressed crystallization but also hindered nitrate photolysis from generating oxidants and reduced the reactivity of glycine. In contrast, some unbonded nitrate existed in deliquescent SN+GC particles to undergo photolysis and triggered glycine decay effectively, though it was significantly hindered once the particle crystallized. Besides glycine, alanine (Ala) was another major FAA in atmospheric particles (mole
250 ratio of Ala to total FAAs = 0.07-0.17) (Matos et al., 2016; Zhu et al., 2020; Zhang et al., 2003). After 8 h irradiation, we also found evident Ala decay in deliquescent SN+Ala particles, but not AN+Ala ones (Figure S8).

It is widely reported that nitrate dominantly exists as SN in the coarse mode aged sea salt particles and AN in the fine mode particles (Zhuang et al., 1999a, b). Concentrations of FAAs in the coarse mode were ~10 times higher than that in the fine
255 mode (Helin et al., 2017), which implies that the FAAs plausibly co-existed with SN in atmospheric particles and subjected to oxidation triggered by effective SN photolysis.

Similar to what we found in SN+GC particles, it has been reported that particulate nitrate photolysis rate constants (i.e., 10^{-5} s^{-1}) can be 2-orders of magnitude higher than nitrate photolysis in cloud and fog water (i.e., 10^{-7} s^{-1}), likely due to the reduced
260 surface cage, etc. (Gen et al., 2022). H_2O_2 photolysis (J = ~2 × 10^{-6} s^{-1}) was considered the primary OH source in aqueous cloud water (Bianco et al., 2015), and the aqueous-phase reactions with OH were reported as an important sink of the cloud FAAs (Wen et al., 2022). However, the small liquid water content in aerosol particles limits the partitioning of H_2O_2 into the

particle phase. Taking particulate [H_2O_2] and [NO_3^-] as 0.1 ng μg^{-1} and 0.2 μg μg^{-1} (per $PM_{2.5}$ mass) (Xuan et al., 2020; Cheng et al., 2016; Li et al., 2022b), respectively, the OH generation from particulate nitrate photolysis could be 4-orders of magnitude higher than from H_2O_2 photolysis. Other oxidants from nitrate photolysis, such as nitrite and HONO, can also react with FAAs to promote their decay, via N-nitration (Kitada et al., 2020). As shown in Figure 3a, the complexation of glycine with the cation could be crucial for allowing free nitrate for photolysis. Other atmospheric cations, such as potassium, magnesium and calcium, can also form complexes with the carboxylic group of amino acids (Case et al., 2020; Lester et al., 2010; Tang et al., 2016). The pH of global ambient aerosol can span from 0-6 (Weber et al., 2016; Liu et al., 2017b), which means that amino acids can exist in both cationic (0<pH<2) and zwitterionic (2<pH<10) forms (Locke et al., 1983; Stroud et al., 1983). Previous studies have reported that complexation is enhanced for cationic amino acids due to the protonation (Moision et al., 2002).

Overall, our work shed light on the potential role of particulate nitrate photolysis in the sink of the atmospheric FAAs, which impacts the cycling of atmospheric organic nitrogen. The reaction rate constants between FAAs and different oxidants from nitrate photolysis can further help quantify the contribution of nitrate photolysis in FAA degradation and improve the prediction of the atmospheric lifetime of FAAs. The reactivity analysis in concentrated systems is complex, and our experimental results can provide valuable data to parameterize the complex thermodynamics in future studies. Systematic studies of the detailed molecular mechanism and the factors influencing nitrate photochemistry and FAA decay, such as molecular configuration, alkalinity, and solvation are recommended. Quantum chemical and molecular dynamic simulations with appropriate parameters would be useful tools for this purpose.

Data availability

Supplementary figures were provided.

Author contributions

ZL and CKC conceptualized the study, ZL, ZC, RZ and YQ performed the experiments and analyzed the data, ZL wrote the manuscript. ZL, ZC, RZ, YQ and CKC reviewed and edited the manuscript.

Competing interests

The authors declare that they have no conflict of interest.

Acknowledgment

We gratefully acknowledge the support from the Hong Kong Research Grants Council (No. 11314222, R1016-20F), and the National Natural Science Foundation of China (No. 42275104, 41905122).

References

Acero, J. L., Stemmler, K., and Von Gunten, U.: Degradation kinetics of atrazine and its degradation products with ozone and OH radicals: a predictive tool for drinking water treatment, Environmental Science & Technology, 34, 591-597, 2000.

300 Aikens, C. M. and Gordon, M. S.: Incremental Solvation of Nonionized and Zwitterionic Glycine, Journal of the American Chemical Society, 128, 12835-12850, 10.1021/ja062842p, 2006.

Asher, S. A., Tuschel, D. D., Vargson, T. A., Wang, L., and Geib, S. J.: Solid state and solution nitrate photochemistry: photochemical evolution of the solid state lattice, The Journal of Physical Chemistry A, 115, 4279-4287, 2011.

Ashraf, H., Guo, Y., Wang, N., Pang, S., and Zhang, Y.-H.: Hygroscopicity of Hofmeister Salts and Glycine Aerosols–Salt Specific Interactions, The Journal of Physical Chemistry A, 125, 1589-1597, 10.1021/acs.jpca.0c10710, 2021.

305 Aziz, E. F., Ottosson, N., Eisebitt, S., Eberhardt, W., Jagoda-Cwiklik, B., Vácha, R., Jungwirth, P., and Winter, B.: Cation-Specific Interactions with Carboxylate in Amino Acid and Acetate Aqueous Solutions: X-ray Absorption and ab initio Calculations, The Journal of Physical Chemistry B, 112, 12567-12570, 10.1021/jp805177v, 2008.

Benedict, K. B., McFall, A. S., and Anastasio, C.: Quantum yield of nitrite from the photolysis of aqueous nitrate above 300 nm, Environmental science & technology, 51, 4387-4395, 2017.

310 Berger, P., Karpel Vel Leitner, N., Doré, M., and Legube, B.: Ozone and hydroxyl radicals induced oxidation of glycine, Water Research, 33, 433-441, https://doi.org/10.1016/S0043-1354(98)00230-9, 1999.

Bianco, A., Passananti, M., Perroux, H., Voyard, G., Mouchel-Vallon, C., Chaumerliac, N., Mailhot, G., Deguillaume, L., and Brigante, M.: A better understanding of hydroxyl radical photochemical sources in cloud waters collected at the puy de Dôme station – experimental versus modelled formation rates, Atmos. Chem. Phys., 15, 9191-9202, 10.5194/acp-15-9191-2015, 315 2015.

Buxton, G. V., Greenstock, C. L., Helman, W. P., and Ross, A. B.: Critical Review of rate constants for reactions of hydrated electrons, hydrogen atoms and hydroxyl radicals (·OH/·O− in Aqueous Solution, Journal of Physical and Chemical Reference Data, 17, 513-886, 10.1063/1.555805, 1988.

Case, D. R., Zubieta, J., and P. Doyle, R.: The Coordination Chemistry of Bio-Relevant Ligands and Their Magnesium 320 Complexes, Molecules, 25, 3172, 2020.

Chan, C. K. and Yao, X.: Air pollution in mega cities in China, Atmospheric Environment, 42, 1-42, 10.1016/j.atmosenv.2007.09.003, 2008.

Chan, M. N., Choi, M. Y., Ng, N. L., and Chan, C. K.: Hygroscopicity of Water-Soluble Organic Compounds in Atmospheric Aerosols: Amino Acids and Biomass Burning Derived Organic Species, Environmental Science & Technology, 39, 1555-325 1562, 10.1021/es049584l, 2005.

Cheng, Z., Luo, L., Wang, S., Wang, Y., Sharma, S., Shimadera, H., Wang, X., Bressi, M., de Miranda, R. M., Jiang, J., Zhou, W., Fajardo, O., Yan, N., and Hao, J.: Status and characteristics of ambient PM2.5 pollution in global megacities, Environment International, 89-90, 212-221, https://doi.org/10.1016/j.envint.2016.02.003, 2016.

Clegg, S. L., Brimblecombe, P., and Wexler, A. S.: Thermodynamic model of the system H+− NH4+− Na+− SO42-− NO3-− 330 Cl-− H2O at 298.15 K, The Journal of Physical Chemistry A, 102, 2155-2171, 1998.

Craig, R. L., Peterson, P. K., Nandy, L., Lei, Z., Hossain, M. A., Camarena, S., Dodson, R. A., Cook, R. D., Dutcher, C. S., and Ault, A. P.: Direct determination of aerosol pH: Size-resolved measurements of submicrometer and supermicrometer aqueous particles, Analytical chemistry, 90, 11232-11239, 2018.

De Haan, D. O., Hawkins, L. N., Kononenko, J. A., Turley, J. J., Corrigan, A. L., Tolbert, M. A., and Jimenez, J. L.: Formation of Nitrogen-Containing Oligomers by Methylglyoxal and Amines in Simulated Evaporating Cloud Droplets, Environmental Science & Technology, 45, 984-991, 10.1021/es102933x, 2011.

Furić, K., Mohaček, V., Bonifačić, M., and Štefanić, I.: Raman spectroscopic study of H2O and D2O water solutions of glycine, Journal of Molecular Structure, 267, 39-44, https://doi.org/10.1016/0022-2860(92)87006-H, 1992.

Gao, S., Xu, B., Zheng, X., Wan, X., Zhang, X., Wu, G., and Cong, Z.: Developing an analytical method for free amino acids in atmospheric precipitation using gas chromatography coupled with mass spectrometry, Atmospheric Research, 256, 105579, 2021.

Gen, M., Liang, Z., Zhang, R., Go Mabato, B. R., and Chan, C. K.: Particulate nitrate photolysis in the atmosphere, Environmental Science: Atmospheres, 10.1039/D1EA00087J, 2022.

Gen, M., Zhang, R., Huang, D. D., Li, Y., and Chan, C. K.: Heterogeneous SO2 Oxidation in Sulfate Formation by Photolysis of Particulate Nitrate, Environmental Science & Technology Letters, 6, 86-91, 10.1021/acs.estlett.8b00681, 2019.

George, C., Ammann, M., D'Anna, B., Donaldson, D. J., and Nizkorodov, S. A.: Heterogeneous photochemistry in the atmosphere, Chem Rev, 115, 4218-4258, 10.1021/cr500648z, 2015.

Gujarati, V. P., Deshpande, M., Patel, K., and Chaki, S.: Comparitive study of nonlinear semi-organic crystals; glycine sodium nitrate, International Letters of Chemistry, Physics and Astronomy, 61, 13, 2015.

Guo, J., Zhou, L., Zen, A., Michaelides, A., Wu, X., Wang, E., Xu, L., and Chen, J.: Hydration of NH_{4}^{+} in Water: Bifurcated Hydrogen Bonding Structures and Fast Rotational Dynamics, Physical Review Letters, 125, 106001, 10.1103/PhysRevLett.125.106001, 2020.

Guo, X., Xiao, H.-S., Wang, F., and Zhang, Y.-H.: Micro-Raman and FTIR spectroscopic observation on the phase transitions of MnSO4 droplets and ionic interactions between Mn2+ and SO42−, The Journal of Physical Chemistry A, 114, 6480-6486, 2010.

Ha, Z. and Chan, C. K.: The Water Activities of MgCl2, Mg(NO3)2, MgSO4, and Their Mixtures, Aerosol Science and Technology, 31, 154-169, 10.1080/027868299304219, 1999.

Haan, D. O. D., Corrigan, A. L., Smith, K. W., Stroik, D. R., Turley, J. J., Lee, F. E., Tolbert, M. A., Jimenez, J. L., Cordova, K. E., and Ferrell, G. R.: Secondary Organic Aerosol-Forming Reactions of Glyoxal with Amino Acids, Environmental Science & Technology, 43, 2818-2824, 10.1021/es803534f, 2009.

Helin, A., Sietiö, O. M., Heinonsalo, J., Bäck, J., Riekkola, M. L., and Parshintsev, J.: Characterization of free amino acids, bacteria and fungi in size-segregated atmospheric aerosols in boreal forest: seasonal patterns, abundances and size distributions, Atmos. Chem. Phys., 17, 13089-13101, 10.5194/acp-17-13089-2017, 2017.

Hu, W., Wang, Z., Huang, S., Ren, L., Yue, S., Li, P., Xie, Q., Zhao, W., Wei, L., and Ren, H.: Biological aerosol particles in polluted regions, Current pollution reports, 6, 65-89, 2020.

Ishizuka, S., Reich, O., David, G., and Signorell, R.: Photo-Induced Shrinking of Aqueous Glycine Aerosol Droplets, Atmos. Chem. Phys. Discuss., 2023, 1-16, 10.5194/acp-2023-6, 2023.

Jentzsch, P. V., Kampe, B., Ciobotă, V., Rösch, P., and Popp, J.: Inorganic salts in atmospheric particulate matter: Raman spectroscopy as an analytical tool, Spectrochimica Acta Part A: Molecular and Biomolecular Spectroscopy, 115, 697-708, 2013.

Kitada, K., Suda, Y., and Takenaka, N.: Cyanide Formation in Freezer Stored Foods: Freezing of a Glycine and Nitrite Mixture, Chemical Research in Toxicology, 33, 1809-1814, 10.1021/acs.chemrestox.0c00054, 2020.

Krauklis, I. V., Tulub, A. V., Golovin, A. V., and Chelibanov, V. P.: Raman Spectra of Glycine and Their Modeling in Terms of the Discrete–Continuum Model of Their Water Solvation Shell, Optics and Spectroscopy, 128, 1598-1601, 10.1134/S0030400X20100161, 2020.

Kristensson, A., Rosenørn, T., and Bilde, M.: Cloud droplet activation of amino acid aerosol particles, The Journal of Physical Chemistry A, 114, 379-386, 2010.

Kumar, S., Rai, A. K., Singh, V. B., and Rai, S. B.: Vibrational spectrum of glycine molecule, Spectrochimica Acta Part A: Molecular and Biomolecular Spectroscopy, 61, 2741-2746, https://doi.org/10.1016/j.saa.2004.09.029, 2005.

Lester, G. E., Jifon, J. L., and Makus, D. J.: Impact of potassium nutrition on postharvest fruit quality: Melon (Cucumis melo L) case study, Plant and soil, 335, 117-131, 2010.

Li, X., Zhang, Y., Shi, L., Kawamura, K., Kunwar, B., Takami, A., Arakaki, T., and Lai, S.: Aerosol Proteinaceous Matter in Coastal Okinawa, Japan: Influence of Long-Range Transport and Photochemical Degradation, Environmental Science & Technology, 56, 5256-5265, 10.1021/acs.est.1c08658, 2022a.

Li, Y., Geng, Y., Hu, X., and Yin, X.: Seasonal differences in sources and formation processes of PM2.5 nitrate in an urban environment of North China, Journal of Environmental Sciences, 120, 94-104, https://doi.org/10.1016/j.jes.2021.08.020, 2022b.

Liang, Z., Chu, Y., Gen, M., and Chan, C. K.: Single-particle Raman spectroscopy for studying physical and chemical processes of atmospheric particles, Atmos. Chem. Phys., 22, 3017-3044, 10.5194/acp-22-3017-2022, 2022a.

Liang, Z., Zhang, R., Gen, M., Chu, Y., and Chan, C. K.: Nitrate Photolysis in Mixed Sucrose–Nitrate–Sulfate Particles at Different Relative Humidities, The Journal of Physical Chemistry A, 125, 3739-3747, 10.1021/acs.jpca.1c00669, 2021.

Liang, Z., Chan, W. L., Tian, X., Lai, A. C. K., Lee, P. K. H., and Chan, C. K.: Inactivation of Escherichia coli in droplets at different ambient relative humidities: Effects of phase transition, solute and cell concentrations, Atmospheric Environment, 280, 119066, https://doi.org/10.1016/j.atmosenv.2022.119066, 2022b.

Liang, Z., Zhou, L., Infante Cuevas, R. A., Li, X., Cheng, C., Li, M., Tang, R., Zhang, R., Lee, P. K. H., Lai, A. C. K., and Chan, C. K.: Sulfate Formation in Incense Burning Particles: A Single-Particle Mass Spectrometric Study, Environmental Science & Technology Letters, 9, 718-725, 10.1021/acs.estlett.2c00492, 2022c.

Lightstone, J. M., Onasch, T. B., Imre, D., and Oatis, S.: Deliquescence, efflorescence, and water activity in ammonium nitrate and mixed ammonium nitrate/succinic acid microparticles, The Journal of Physical Chemistry A, 104, 9337-9346, 2000.

400 Ling, T. Y. and Chan, C. K.: Formation and Transformation of Metastable Double Salts from the Crystallization of Mixed Ammonium Nitrate and Ammonium Sulfate Particles, Environmental Science & Technology, 41, 8077-8083, 10.1021/es071419t, 2007.

Liu, F., Lai, S., Tong, H., Lakey, P. S., Shiraiwa, M., Weller, M. G., Pöschl, U., and Kampf, C. J.: Release of free amino acids upon oxidation of peptides and proteins by hydroxyl radicals, Analytical and bioanalytical chemistry, 409, 2411-2420, 2017a.

405 Liu, M., Song, Y., Zhou, T., Xu, Z., Yan, C., Zheng, M., Wu, Z., Hu, M., Wu, Y., and Zhu, T.: Fine particle pH during severe haze episodes in northern China, Geophysical Research Letters, 44, 5213-5221, 2017b.

Locke, M. J. and McIver Jr, R. T.: Effect of solvation on the acid/base properties of glycine, Journal of the American Chemical Society, 105, 4226-4232, 1983.

Marsh, A., Miles, R. E., Rovelli, G., Cowling, A. G., Nandy, L., Dutcher, C. S., and Reid, J. P.: Influence of organic compound
410 functionality on aerosol hygroscopicity: dicarboxylic acids, alkyl-substituents, sugars and amino acids, Atmospheric Chemistry and Physics, 17, 5583-5599, 2017.

Matos, J. T., Duarte, R. M., and Duarte, A. C.: Challenges in the identification and characterization of free amino acids and proteinaceous compounds in atmospheric aerosols: A critical review, TrAC Trends in Analytical Chemistry, 75, 97-107, 2016.

Matsumoto, K., Kim, S., and Hirai, A.: Origins of free and combined amino acids in the aerosols at an inland urban site in
415 Japan, Atmospheric Environment, 259, 118543, https://doi.org/10.1016/j.atmosenv.2021.118543, 2021.

Matsumura, T. and Hayashi, M.: Hygroscopic Growth of an (NH 4) 2 SO 4 Aqueous Solution Droplet Measured Using an Environmental Scanning Electron Microscope (ESEM), Aerosol Science and Technology, 41, 770-774, 10.1080/02786820701436831, 2007.

Medoš, Ž., Plechkova, N. V., Friesen, S., Buchner, R., and Bešter-Rogač, M.: Insight into the Hydration of Cationic
420 Surfactants: A Thermodynamic and Dielectric Study of Functionalized Quaternary Ammonium Chlorides, Langmuir, 35, 3759-3772, 10.1021/acs.langmuir.8b03993, 2019.

Moision, R. M. and Armentrout, P. B.: Experimental and Theoretical Dissection of Sodium Cation/Glycine Interactions, The Journal of Physical Chemistry A, 106, 10350-10362, 10.1021/jp0216373, 2002.

Mopper, K. and Zika, R. G.: Free amino acids in marine rains: evidence for oxidation and potential role in nitrogen cycling,
425 Nature, 325, 246-249, 1987.

Pei, W.-X., Ma, S.-S., Chen, Z., Zhu, Y., Pang, S.-F., and Zhang, Y.-H.: Heterogeneous uptake of NO2 by sodium acetate droplets and secondary nitrite aerosol formation, Journal of Environmental Sciences, https://doi.org/10.1016/j.jes.2022.05.048, 2022.

Philipsen, P., Knudsen, L., Gniadecka, M., Ravnbak, M., and Wulf, H.: Diagnosis of malignant melanoma and basal cell
430 carcinoma by in vivo NIR-FT Raman spectroscopy is independent of skin pigmentation, Photochemical & Photobiological Sciences, 12, 770-776, 2013.

Ren, L., Bai, H., Yu, X., Wu, F., Yue, S., Ren, H., Li, L., Lai, S., Sun, Y., Wang, Z., and Fu, P.: Molecular composition and seasonal variation of amino acids in urban aerosols from Beijing, China, Atmospheric Research, 203, 28-35, https://doi.org/10.1016/j.atmosres.2017.11.032, 2018.

435   Scharko, N. K., Berke, A. E., and Raff, J. D.: Release of nitrous acid and nitrogen dioxide from nitrate photolysis in acidic aqueous solutions, Environmental science & technology, 48, 11991-12001, 2014.

Selvarani, K., Mahalakshmi, R., and Srinivasan, N.: Growth and characterization of nonlinear optical crystal glycine sodium nitrate and its biological activity, Journal of Materials Science: Materials in Electronics, 33, 13408-13417, 2022.

Socrates, G.: Infrared and Raman characteristic group frequencies: tables and charts, John Wiley & Sons2004.

440   Song, T., Wang, S., Zhang, Y., Song, J., Liu, F., Fu, P., Shiraiwa, M., Xie, Z., Yue, D., Zhong, L., Zheng, J., and Lai, S.: Proteins and Amino Acids in Fine Particulate Matter in Rural Guangzhou, Southern China: Seasonal Cycles, Sources, and Atmospheric Processes, Environmental Science & Technology, 51, 6773-6781, 10.1021/acs.est.7b00987, 2017.

Stroud, E. D., Fife, D. J., and Smith, G. G.: A method for the determination of the pKa of the. alpha.-hydrogen in amino acids using racemization and exchange studies, The Journal of Organic Chemistry, 48, 5368-5369, 1983.

445   Suresh, S., Ramanand, A., Mani, P., and Murthyanand, K.: Growth, structural, optical, mechanical and dielectric properties of glycine sodium nitrate (GSN) single crystal, Journal of optoelectronics and Biomedical Materials, 1, 129-139, 2010.

Surovtsev, N., Adichtchev, S., Malinovsky, V., Ogienko, A., Drebushchak, V., Manakov, A. Y., Ancharov, A., Yunoshev, A., and Boldyreva, E.: Glycine phases formed from frozen aqueous solutions: Revisited, The Journal of chemical physics, 137, 065103, 2012.

450   Tang, I. N.: Thermodynamic and optical properties of mixed-salt aerosols of atmospheric importance, Journal of Geophysical Research: Atmospheres, 102, 1883-1893, https://doi.org/10.1029/96JD03085, 1997.

Tang, N. and Skibsted, L. H.: Calcium Binding to Amino Acids and Small Glycine Peptides in Aqueous Solution: Toward Peptide Design for Better Calcium Bioavailability, Journal of Agricultural and Food Chemistry, 64, 4376-4389, 10.1021/acs.jafc.6b01534, 2016.

455   Tortonda, F. R., Pascual-Ahuir, J. L., Silla, E., and Tuñón, I.: Why is glycine a zwitterion in aqueous solution? A theoretical study of solvent stabilising factors, Chemical Physics Letters, 260, 21-26, https://doi.org/10.1016/0009-2614(96)00839-1, 1996.

Venkatesu, P., Lee, M.-J., and Lin, H.-m.: Densities of aqueous solutions containing model compounds of amino acids and ionic salts at T=298.15K, The Journal of Chemical Thermodynamics, 39, 1206-1216, 460   https://doi.org/10.1016/j.jct.2006.11.014, 2007.

Vimalan, M., Flora, X. H., Tamilselvan, S., Jeyasekaran, R., Sagayaraj, P., and Mahadevan, C.: Optical, thermal, mechanical and electrical properties of a new NLO material: Mono-L-alaninium nitrate (MAN), Arch Phys Res, 1, 44-53, 2010.

Wang, N., Guo, Y., Li, J., Pang, S., and Zhang, Y.: Hygroscopic behavior and phase state of mixed NH4NO3 /amino acids particles by microscopy and IR technology, Atmospheric Environment, 273, 118951, 465   https://doi.org/10.1016/j.atmosenv.2022.118951, 2022.

Wang, P., Wang, N., Pang, S.-F., and Zhang, Y.-H.: Hygroscopicity of internally mixed particles glycine/NaNO3 studied by FTIR-ATR technique, Journal of Aerosol Science, 116, 25-33, https://doi.org/10.1016/j.jaerosci.2017.11.013, 2018.

Weber, R. J., Guo, H., Russell, A. G., and Nenes, A.: High aerosol acidity despite declining atmospheric sulfate concentrations over the past 15 years, Nature Geoscience, 9, 282-285, 2016.

470   Wen, L., Schaefer, T., Zhang, Y., He, L., Ventura, O. N., and Herrmann, H.: T- and pH-dependent OH radical reaction kinetics with glycine, alanine, serine, and threonine in the aqueous phase, Physical Chemistry Chemical Physics, 24, 11054-11065, 10.1039/D1CP05186E, 2022.

Xu, Y., Wu, D., Xiao, H., and Zhou, J.: Dissolved hydrolyzed amino acids in precipitation in suburban Guiyang, southwestern China: Seasonal variations and potential atmospheric processes, Atmospheric Environment, 211, 247-255, 2019.

475   Xuan, X., Chen, Z., Gong, Y., Shen, H., and Chen, S.: Partitioning of hydrogen peroxide in gas-liquid and gas-aerosol phases, Atmos. Chem. Phys., 20, 5513-5526, 10.5194/acp-20-5513-2020, 2020.

Zhang, Q. and Anastasio, C.: Free and combined amino compounds in atmospheric fine particles (PM2.5) and fog waters from Northern California, Atmospheric Environment, 37, 2247-2258, https://doi.org/10.1016/S1352-2310(03)00127-4, 2003.

Zhang, R., Gen, M., Fu, T.-M., and Chan, C. K.: Production of Formate via Oxidation of Glyoxal Promoted by Particulate
480   Nitrate Photolysis, Environmental Science & Technology, 55, 5711-5720, 10.1021/acs.est.0c08199, 2021.

Zhang, R., Gen, M., Liang, Z., Li, Y. J., and Chan, C. K.: Photochemical Reactions of Glyoxal during Particulate Ammonium Nitrate Photolysis: Brown Carbon Formation, Enhanced Glyoxal Decay, and Organic Phase Formation, Environmental Science & Technology, 56, 1605-1614, 10.1021/acs.est.1c07211, 2022.

Zhu, R.-g., Xiao, H.-Y., Zhu, Y., Wen, Z., Fang, X., and Pan, Y.: Sources and Transformation Processes of Proteinaceous
485   Matter and Free Amino Acids in PM2.5, Journal of Geophysical Research: Atmospheres, 125, e2020JD032375, https://doi.org/10.1029/2020JD032375, 2020.

Zhu, R.-G., Xiao, H.-Y., Luo, L., Xiao, H., Wen, Z., Zhu, Y., Fang, X., Pan, Y., and Chen, Z.: Measurement report: Hydrolyzed amino acids in fine and coarse atmospheric aerosol in Nanchang, China: concentrations, compositions, sources and possible bacterial degradation state, Atmospheric Chemistry and Physics, 21, 2585-2600, 2021.

490   Zhuang, H., Chan, C. K., Fang, M., and Wexler, A. S.: Size distributions of particulate sulfate, nitrate, and ammonium at a coastal site in Hong Kong, Atmospheric Environment, 33, 843-853, https://doi.org/10.1016/S1352-2310(98)00305-7, 1999a.

Zhuang, H., Chan, C. K., Fang, M., and Wexler, A. S.: Formation of nitrate and non-sea-salt sulfate on coarse particles, Atmospheric Environment, 33, 4223-4233, https://doi.org/10.1016/S1352-2310(99)00186-7, 1999b.

Zuend, A., Marcolli, C., Booth, A., Lienhard, D. M., Soonsin, V., Krieger, U., Topping, D. O., McFiggans, G., Peter, T., and
495   Seinfeld, J. H.: New and extended parameterization of the thermodynamic model AIOMFAC: calculation of activity coefficients for organic-inorganic mixtures containing carboxyl, hydroxyl, carbonyl, ether, ester, alkenyl, alkyl, and aromatic functional groups, Atmospheric Chemistry and Physics, 11, 9155-9206, 2011.
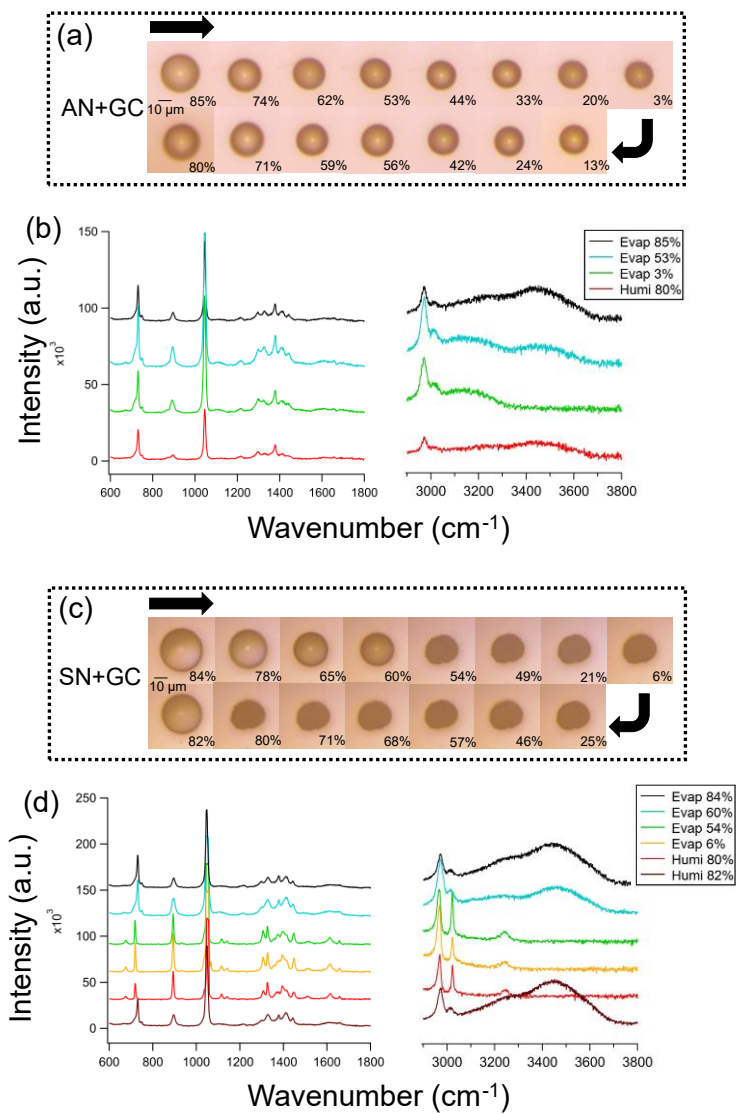
Figure 1. Images and Raman spectra of the mixed (a, b) AN+GC particles and (c, d) SN+GC particles during an evaporation-humidification cycle. The arrows in a and c show the changes of relative humidity.

500

505

510
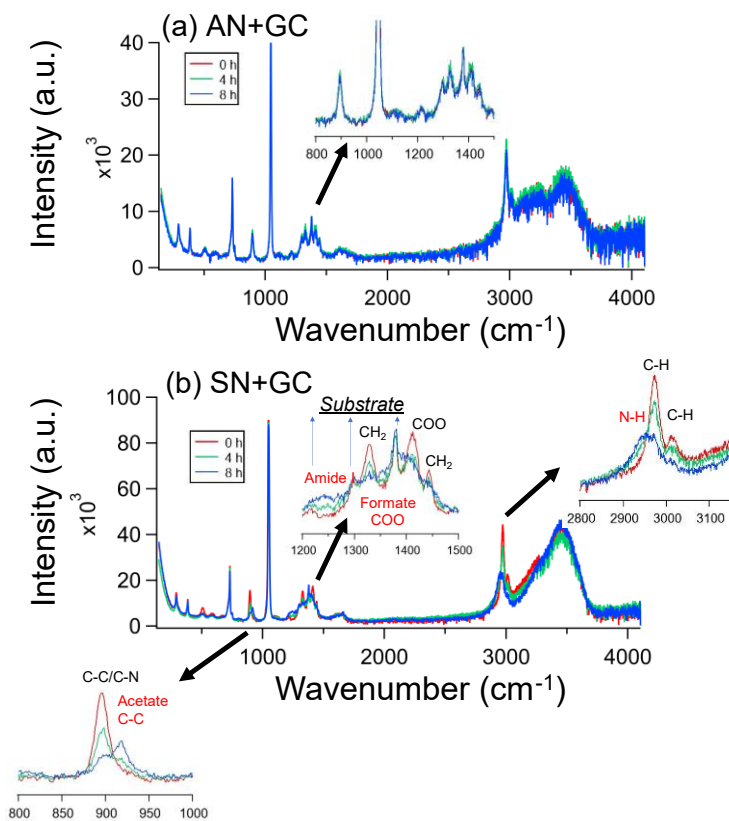
515

Figure 2. Raman spectral evolution of (a) AN+GC and (b) SN+GC particles after 0-, 4-, and 8-hours irradiation. Insets are expanded regions of the SN+GC particle spectra in the ranges of [860, 960], [1150, 1600], and [2800, 3150] (unit: cm^{-1}). The red annotations denote the peaks from products. The spectra were normalized by the substrate peak at around 1400 cm^{-1}.

520

525
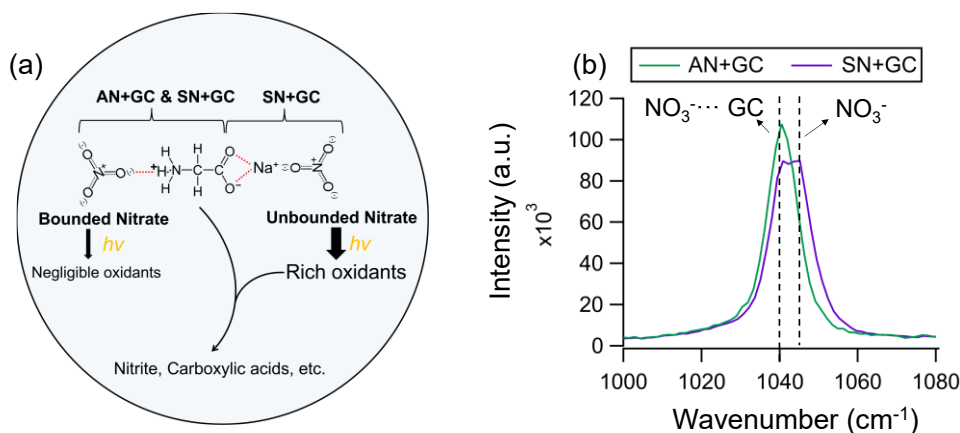
Figure 3. (a) A plausible schematic of the photochemical processes and molecular interactions in AN+GC and SN+GC particles. Red dashed lines indicate the binding. The binding between AN+GC may be mediated by water (Ashraf et al., 2021). (b) The Raman peak of nitrate of AN+GC and SN+GC particles at 80% RH before illumination. The spectra were normalized by the substrate peaks.
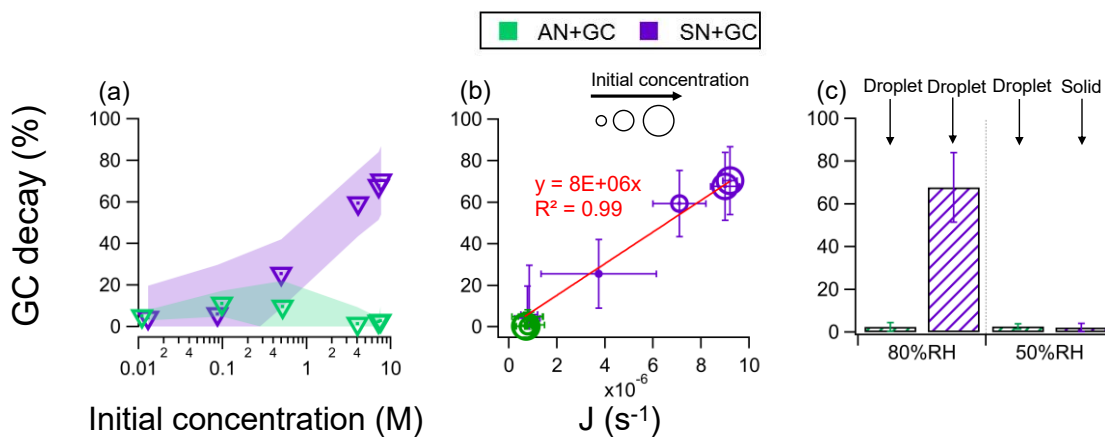
Figure 4. (a) The percentage decay of GC as a function of the initial concentration of GC in AN+GC and SN+GC equimolar mixtures. The shade regions represent the standard deviations. (b) The correlation between nitrate photolysis rate constant (J) and the percentage GC decay. (c) The percentage GC decay in AN+GC and SN+GC particles at 80% and 50% RH.